YAP/TAZ mediate TGFβ2-induced Schlemm's canal cell dysfunction

Haiyan Li[a,b,†], Ayushi Singh[a,b], Kristin M. Perkumas[c], W. Daniel Stamer[c,d], Preethi S. Ganapathy[a,e,g], Samuel Herberg[a,b,f,g,h*]

Affiliations:

[a] Department of Ophthalmology and Visual Sciences, SUNY Upstate Medical University, Syracuse, NY 13210, USA

[b] Department of Cell and Developmental Biology, SUNY Upstate Medical University, Syracuse, NY 13210, USA

[c] Department of Ophthalmology, Duke Eye Center, Duke University, Durham, NC 27708, USA

[d] Department of Biomedical Engineering, Duke University, Durham, NC 27708, USA

[e] Department of Neuroscience and Physiology, SUNY Upstate Medical University, Syracuse, NY 13210, USA

[f] Department of Biochemistry and Molecular Biology, SUNY Upstate Medical University, Syracuse, NY 13210, USA

[g] BioInspired Institute, Syracuse University, Syracuse, NY 13244, USA

[h] Department of Biomedical and Chemical Engineering, Syracuse University, Syracuse, NY 13244, USA

[†]Present address: Wallace H. Coulter Department of Biomedical Engineering, Georgia Institute of Technology & Emory University, Atlanta, GA 30332, USA

*To whom correspondence should be addressed: Samuel Herberg, PhD, Assistant Professor; Department of Ophthalmology and Visual Sciences, SUNY Upstate Medical University, 505 Irving Avenue, Neuroscience Research Building Room 4609, Syracuse, NY 13210, USA, email: herbergs@upstate.edu

Keywords: POAG, mechanotransduction, TM stiffness, hydrogel, actin cytoskeleton

34 **Abstract**

35 **Purpose:** Elevated transforming growth factor beta2 (TGFβ2) levels in the aqueous humor have
36 been linked to glaucomatous outflow tissue dysfunction. Potential mediators of dysfunction are
37 the transcriptional co-activators, Yes-associated protein (YAP) and transcriptional coactivator
38 with PDZ binding motif (TAZ). However, the molecular underpinnings of YAP/TAZ modulation
39 in Schlemm's Canal (SC) cells under glaucomatous conditions are not well understood. Here, we
40 investigate how TGFβ2 regulates YAP/TAZ activity in human SC (HSC) cells using biomimetic
41 extracellular matrix (ECM) hydrogels, and examine whether pharmacologic YAP/TAZ inhibition
42 would attenuate TGFβ2-induced HSC cell dysfunction.

43 **Methods:** Primary HSC cells were seeded atop photocrosslinked ECM hydrogels, made of
44 collagen type I, elastin-like polypeptide and hyaluronic acid, or encapsulated within the hydrogels.
45 HSC cells were induced with TGFβ2 in the absence or presence of concurrent actin destabilization
46 or pharmacologic YAP/TAZ inhibition. Changes in actin cytoskeletal organization, YAP/TAZ
47 activity, ECM production, phospho-myosin light chain levels, and hydrogel contraction were
48 assessed.

49 **Results:** TGFβ2 significantly increased YAP/TAZ nuclear localization in HSC cells, which was
50 prevented by either filamentous (F)-actin relaxation or depolymerization. Pharmacologic
51 YAP/TAZ inhibition using verteporfin without light stimulation decreased fibronectin expression
52 and reduced actomyosin cytoskeletal rearrangement in HSC cells induced by TGFβ2. Similarly,
53 verteporfin significantly attenuated TGFβ2-induced HSC cell-encapsulated hydrogel contraction.

54 **Conclusions:** Our data provide evidence for a pathologic role of aberrant YAP/TAZ signaling in
55 HSC cells under simulated glaucomatous conditions, and suggest that pharmacologic YAP/TAZ
56 inhibition has promising potential to improve outflow tissue dysfunction.

57 **Introduction**

58 The Schlemm's canal (SC) is a continuous vessel that encircles the anterior chamber at the
59 iridocorneal angle; its lumen is lined with a single non-fenestrated layer of endothelial cells having
60 both blood and lymphatic characteristics [1-5]. Situated in close apposition to the trabecular
61 meshwork (TM), the SC is divided into the inner and outer wall [2]. The SC inner wall experiences
62 a basal-to-apical pressure gradient (intraocular versus episcleral venous pressures) that drives
63 aqueous humor into the SC lumen, which is then drained into the collector channels and aqueous
64 veins [6]. Most of the resistance to aqueous humor outflow is generated at, or close to the SC inner
65 wall in a region called the juxtacanalicular tissue (JCT) of the TM [7-9]. Importantly, increased
66 outflow resistance in the JCT leads to elevated intraocular pressure (IOP), the only modifiable risk
67 factor for primary open-angle glaucoma (POAG) [8,10-13].

68 Previous studies have demonstrated that glaucomatous SC cells isolated from POAG eyes
69 exhibited higher levels of filamentous (F)-actin, α-smooth muscle actin (αSMA), and fibronectin,
70 as well as increased cell stiffness compared to normal SC cells [14,15]. The ocular hypertension-
71 causing steroid dexamethasone was shown to increase F-actin fibers, while the IOP-lowering Rho-
72 associated kinase (ROCK) inhibitor Y27632 decreased F-actin levels [16,17]; F-actin is thought to
73 mediate SC cell contractility and stiffness to negatively affect aqueous humor outflow and IOP [18].
74 Thus, SC cell dysfunction is thought to be a significant contributor to the increased outflow
75 resistance in POAG; however, the mechanistic underpinnings of SC cell pathobiology remain
76 incompletely understood.

77 Transforming growth factor beta 2 (TGFβ2), the predominant TGFβ isoform in the eye and
78 aqueous humor, is a major player in contributing to the pathologic changes in POAG [10,19-23]. It has
79 been shown that levels of TGFβ2 are elevated in eyes of glaucoma patients compared to age-

80 matched normal eyes [21,22,24,25]. In culture, TM and SC cells isolated from donor eyes with POAG
81 secrete more active TGFβ2 protein compared to normal cells [15,26]. Accordingly, perfusion of
82 TGFβ2 in human anterior segments increases resistance in the conventional outflow pathway [27].
83 At the cellular level, TGFβ2 increases actin stress fibers and phospho-myosin light chain (p-MLC)
84 to drive pathologic TM cell contraction [28-30]. Moreover, exposure of TM cells to TGFβ2 induces
85 the expression/deposition of extracellular matrix (ECM) proteins such as collagen types I and IV,
86 and fibronectin [28,31-33]. Despite the progress made in uncovering the role of TGFβ2 in TM cell
87 dysfunction, the contributions of TGFβ2 to SC cell pathobiology are less well understood.

88 Yes-associated protein (YAP) and transcriptional coactivator with PDZ-binding motif (TAZ)
89 are powerful regulators of cell proliferation and differentiation, with an established link to tissue
90 fibrosis [34-38]. Upon nuclear translocation, YAP/TAZ interact with TEA domain (TEAD)
91 transcription factors to drive the expression of known (CTGF, CYR61, ANKRD1) and glaucoma-
92 related putative downstream effectors of active YAP/TAZ signaling (e.g., transglutaminase-2
93 (TGM2)) [39]. To that end, *YAP1* was recently identified among a group of previously unknown
94 POAG risk loci across European, Asian, and African ancestries, suggesting a potential causal
95 association with outflow dysfunction [40]. YAP/TAZ can be activated by multiple stimuli, such as
96 stiffened ECM, increased mechanical stress, and exposure to growth factors [41,42]. Recently, we
97 demonstrated that both ECM stiffening and TGFβ2 increase YAP/TAZ activity in human TM cells,
98 which was linked to pathologic cell contractility and ECM remodeling that may exacerbate
99 glaucoma pathology [26].

100 The physiological substrate of the SC inner wall endothelial cells is its discontinuous basal
101 lamina, which is in direct contact with the JCT of the TM [3,6]. Recently, we developed a
102 bioengineered hydrogel composed of ECM biopolymers found in the native JCT region

103 encapsulated with human TM (HTM) cells, and demonstrated its utility for studying cell-ECM
104 interactions under normal and simulated glaucomatous conditions in a relevant tissue-mimetic 3D
105 microenvironment [26,30,43]. Here, we investigated the effects of TGFβ2 on regulating YAP/TAZ
106 activity in primary human SC cells cultured atop the acellular ECM hydrogel. Additionally, we
107 examined whether pharmacologic YAP/TAZ inhibition would alleviate TGFβ2-induced cell
108 dysfunction.
109

110 **Materials and Methods**

111 ***HSC cell isolation and culture***

112 Experiments using human donor eye tissue were approved by the SUNY Upstate Medical
113 University Institutional Review Board (protocol #1211036), and were performed in accordance
114 with the tenets of the Declaration of Helsinki for the use of human tissue. Primary human SC (HSC)
115 cells were isolated from healthy donor corneal rims discarded after transplant surgery and cultured
116 according to established protocols [5]. Briefly, the corneal rims were cut into wedges and placed into
117 a 100 mm dish containing low-glucose Dulbecco's Modified Eagle's Medium (DMEM; Gibco;
118 Thermo Fisher Scientific, Waltham, MA, USA) with 10% fetal bovine serum (FBS; Atlanta
119 Biologicals, Flowery Branch, GA, USA) and 1% penicillin/streptomycin/glutamine (PSG; Gibco).
120 Using an SMZ1270 stereomicroscope (Nikon Instruments, Melville, NY, USA), a 2% gelatin-
121 coated (Sigma-Aldrich) 6-0 nylon monofilament sterile suture (eSutures, Mokena, IL, USA) was
122 inserted into the SC lumen of each wedge with fine-tipped forceps (Fine Science Tools, Foster
123 City, CA, USA), and these wedges were cultured in DMEM with 10% FBS and 1% PSG, and
124 maintained at 37°C in a humidified atmosphere with 5% CO_2 for 3 weeks. Next, curvilinear
125 incisions were made parallel to Schwalbe's line (alongside the suture) into the TM, which

126 produced a TM flap. After lifting the TM, the sutures were gently removed, and a ~2 mm long
127 piece was cut from each end of the suture to prevent fibrotic cell contamination. Next, the sutures
128 were washed with Dulbecco's Phosphate Buffered Saline (DPBS; Gibco), placed into a single well
129 of gelatin-coated (Sigma-Aldrich) 6-well culture plates (Corning; Thermo Fisher Scientific), and
130 digested for 2 min with 0.25% trypsin/0.5 mM EDTA (Gibco). Subsequently, 5 ml DMEM with
131 10% FBS and 1% PSG were added, and the sutures were moved to another gelatin-coated well.
132 The digests and sutures were cultured in DMEM with 10% FBS and 1% PSG, and maintained at
133 37°C in a humidified atmosphere with 5% CO_2. Fresh media was supplied every 2-3 days. Once
134 confluent, HSC cells were lifted with 0.25% trypsin/0.5 mM EDTA and sub-cultured in DMEM
135 with 10% FBS and 1% PSG. All studies were conducted using cells passage 3-6. Four HSC cell
136 strains (HSC01, HSC02, HSC03, HSC09) were characterized and used for the experiments herein;
137 the reference cell strain HSC78 was isolated and characterized at Duke University by K.M.P. and
138 W.D.S. (**Table 1**). Different combinations of 3 HSC cell strains were used per experiment,
139 depending on cell availability.

140 **Table 1: HSC cell strain information.**

ID	Sex	Age
HSC01	Male	33
HSC02	Male	46
HSC03	Female	46
HSC09	Female	69
Reference HSC78*	Male	77
Reference HSC88*	Female	67
**obtained from W.D.S. at Duke University*		

141

142 ***HSC cell characterization***

143 HSC cells were seeded at 1 × 10^4 cells/cm^2 in 6-well culture plates or on sterilized glass
144 coverslips in 24-well culture plates, and cultured in DMEM with 10% FBS and 1% PSG. HSC cell
145 morphology and growth characteristics were monitored by phase contrast microscopy using an
146 LMI-3000 Series Routine Inverted Microscope (Laxco; Thermo Fisher Scientific). Once confluent,
147 monolayers of HSC cells were processed for immunocytochemistry and immunoblot analyses to
148 assess expression of fibulin-2 and vascular endothelial-cadherin, respectively, with human
149 umbilical vein endothelial cells (ATCC, Manassas, VA, USA) serving as a positive control and
150 previously validated HTM cells (HTM01 or HTM19) [43] serving as negative controls. To rule out
151 the contamination of HTM cells, dexamethasone (Fisher Scientific)-induced myocilin expression
152 was assessed in HSC cells. Briefly, confluent HSC cells were treated with 100 nM dexamethasone
153 or vehicle control (0.1% (v/v) ethanol) in DMEM with 1% FBS and 1% PSG for 4 d, and serum-
154 and phenol red-free DMEM for 3 d. The HSC cell culture supernatants were collected and
155 concentrated using Amicon® Ultra Centrifugal Filters (Millipore Sigma, Burlington, MA, USA)
156 for immunoblot analysis.

157

158 ***Preparation of ECM thin-film hydrogels***

159 Hydrogel precursors methacrylate-conjugated bovine collagen type I (MA-COL, Advanced
160 BioMatrix, Carlsbad, CA, USA; 3.6 mg/ml [all final concentrations]), thiol-conjugated hyaluronic
161 acid (SH-HA, Glycosil®, Advanced BioMatrix; 0.5 mg/ml, 0.025% (w/v) photoinitiator Irgacure®
162 2959; Sigma-Aldrich, St. Louis, MO, USA) and in-house expressed elastin-like polypeptide (SH-
163 ELP, thiol via KCTS flanks [43]; 2.5 mg/ml) were thoroughly mixed. Thirty microliters of the
164 hydrogel solution were pipetted onto a Surfasil (Fisher Scientific)-coated 18 × 18-mm square glass

165 coverslip followed by placing a regular 12-mm round glass coverslip onto the hydrogels.
166 Constructs were crosslinked by exposure to UV light (OmniCure S1500 UV Spot Curing System;
167 Excelitas Technologies, Mississauga, Ontario, Canada) at 320-500 nm, 2.2 W/cm^2 for 5 s, as
168 previously described [26,30,43]. The hydrogel-adhered coverslips were removed with fine-tipped
169 tweezers and placed in 24-well culture plates (Corning; Thermo Fisher Scientific). The elastic
170 modulus of the ECM hydrogel was previously measured at ~0.2 kPa [26].
171
172 ***HSC cell treatments***
173 HSC cells were seeded at 2 × 10^4 cells/cm^2 atop premade ECM hydrogels and cultured in
174 DMEM with 10% FBS and 1% PSG for 1 or 2 days. Then, HSC cells were cultured in serum-free
175 DMEM with 1% PSG and subjected to the different treatments: TGFβ2 (2.5 ng/ml; R&D Systems,
176 Minneapolis, MN, USA; for 3 d), the ROCK inhibitor Y27632 (10 μM; Sigma-Aldrich; for 3 d or
177 30 min only), the actin depolymerizer latrunculin B (10 μM; for 30 min only to preserve cell
178 viability; Tocris Bioscience; Thermo Fisher Scientific), or the YAP inhibitor verteporfin (0.5 μM;
179 Sigma-Aldrich; for 3 d).
180
181 ***Immunoblot analysis***
182 Equal protein amounts (10 or 40 μg), determined by standard bicinchoninic acid assay (Pierce;
183 Thermo Fisher Scientific), from concentrated HSC cell culture supernatants ± dexamethasone at 7
184 d or from HSC cell lysates in lysis buffer (radioimmunoprecipitation assay (RIPA) buffer: 150
185 mM sodium chloride, 1.0% Triton™ X-100, 0.5% sodium deoxycholate, 0.1% sodium dodecyl
186 sulfate, 50 mM Tris, pH 8.0; all from Thermo Fisher Scientific) supplemented with Halt™
187 protease/phosphatase inhibitor cocktail (Thermo Fisher Scientific) in 4× loading buffer (Invitrogen;

188 Thermo Fisher Scientific) with 5% beta-mercaptoethanol (Fisher Scientific) were boiled for 5 min,
189 subjected to SDS-PAGE using NuPAGE™ 4-12% Bis-Tris Gels (Invitrogen; Thermo Fisher
190 Scientific) at 120V for 80 min, and transferred to 0.45 µm polyvinylidene difluoride (Sigma;
191 Thermo Fisher Scientific) or 0.2 µm nitrocellulose membranes (Bio-Rad, Hercules, CA, USA).
192 Membranes were blocked with 5% bovine serum albumin (Thermo Fisher Scientific) in tris-
193 buffered saline with 0.2% Tween®20 (Thermo Fisher Scientific), and probed with primary
194 antibodies followed by incubation with HRP-conjugated or fluorescent secondary antibodies (LI-
195 COR, Lincoln, NE, USA). Bound antibodies were visualized with the enhanced chemiluminescent
196 detection system (Pierce) on autoradiography film (Thermo Fisher Scientific) or Odyssey® CLx
197 imager (LI-COR). A list of all antibodies and their working dilutions can be found in
198 **Supplementary Table 1**.
199
200 ***Immunocytochemistry analysis***
201 HSC cells atop ECM hydrogels subjected to the different treatments for 3 d were fixed with 4%
202 paraformaldehyde (Thermo Fisher Scientific) at room temperature for 20 min, permeabilized with
203 0.5% Triton™ X-100 (Thermo Fisher Scientific), blocked with blocking buffer (BioGeneX), and
204 incubated with primary antibodies, followed by incubation with fluorescent secondary antibodies;
205 nuclei were counterstained with 4′,6′-diamidino-2-phenylindole (DAPI; Abcam). Similarly, cells
206 were stained with Phalloidin-iFluor 488 (Invitrogen) or 594 (Abcam)/DAPI according to the
207 manufacturer's instructions. Coverslips were mounted with ProLong™ Gold Antifade (Invitrogen)
208 on Superfrost™ microscope slides (Fisher Scientific), and fluorescent images were acquired with
209 an Eclipse N*i* microscope (Nikon Instruments, Melville, NY, USA). A list of all antibodies and
210 their working dilutions can be found in **Supplementary Table 1**.

211 ***Image analysis***

212 All image analyses were performed using FIJI software (National Institutes of Health (NIH),
213 Bethesda, MD, USA). Briefly, the cytoplasmic YAP/TAZ intensity was measured by subtracting
214 the spatially overlapping nuclear (DAPI) intensity from the total YAP/TAZ intensity. The nuclear
215 YAP/TAZ intensity was recorded as the proportion of total YAP/TAZ intensity that spatially
216 overlapped with the nucleus (DAPI). YAP/TAZ nuclear/cytoplasmic (N/C) ratio was calculated as
217 follows: N/C ratio = (nuclear YAP/TAZ signal/area of nucleus)/(cytoplasmic signal/area of
218 cytoplasm). Fluorescence intensity of F-actin, FN, TGM2, and p-MLC were measured in at least
219 30 images from 3 HSC cell strains with 3 replicates per HSC cell strain with standardized image
220 background subtraction (using species-matched IgG negative controls) using FIJI software. Given
221 the lack of defined αSMA fibers in untreated controls, we quantified the number of cells exhibiting
222 αSMA signal/fibers (i.e., yes/no decision) per image after standardized background correction and
223 calculated % of αSMA-positive cells according to a previous report [44]. At least 150 cells were
224 analyzed in 30 images from 3 HSC cell strains with 3 replicates per HSC cell strain. For each
225 experiment, care was taken to include an equivalent number of cells across groups.

226

227 ***HSC hydrogel contraction analysis.***

228 HSC cell-laden hydrogels were prepared by mixing HSC cells (1.0×10^6 cells/ml) with MA-
229 COL (3.6 mg/ml), SH-HA (0.5 mg/ml, 0.025% (w/v) photoinitiator) and SH-ELP (2.5 mg/ml) on
230 ice, followed by pipetting 10 μl droplets of the HSC cell-laden hydrogel precursor solution onto
231 polydimethylsiloxane (PDMS; Sylgard 184; Dow Corning)-coated 24-well culture plates.
232 Constructs were crosslinked as described above (320-500 nm, 2.2 W/cm^2, 5 s). HSC cell-laden
233 hydrogels were cultured in DMEM with 10% FBS and 1% PSG in presence of the different

234 treatments. Longitudinal brightfield images were acquired at 0 d and 5 d with an Eclipse T*i*
235 microscope (Nikon). Construct area from N = 12 hydrogels per group from 3 HSC cell strains with
236 4 replicates per cell strain was measured using FIJI software and normalized to 0 d followed by
237 normalization to controls.
238
239 ***HSC hydrogel cell viability analysis***
240 Cell viability was measured with the CellTiter 96® Aqueous Non-Radioactive Cell
241 Proliferation Assay (Promega) following the manufacturer's protocol. HSC hydrogels cultured in
242 DMEM with 10% FBS and 1% PSG in presence of the different treatments for 5 d were incubated
243 with the staining solution (38 µl MTS, 2 µl PMS solution, 200 µl DMEM) at 37ºC for 1.5 h.
244 Absorbance at 490 nm was recorded using a spectrophotometer plate reader (BioTek, Winooski,
245 VT, USA). Blank-subtracted absorbance values served as a direct measure of HSC cell viability
246 from N = 12 hydrogels per group from 3 HSC cell strains with 4 replicates per cell strain.
247
248 ***Statistical analysis***
249 Individual sample sizes are specified in each figure caption. Comparisons between groups were
250 assessed by two-way analysis of variance (ANOVA) with Tukey's multiple comparisons *post hoc*
251 tests, as appropriate. The significance level was set at $p<0.05$ or lower. GraphPad Prism software
252 v9.2 (GraphPad Software, La Jolla, CA, USA) was used for all analyses.
253
254

255 **Results**

256 ***HSC cell characterization***

257 Four HSC cell strains (HSC01, HSC02, HSC03, and HSC09) were used and compared to
258 validated reference strains (HSC78 and HSC88). All of our HSC cell strains exhibited typical
259 spindle-like elongated cell morphology comparable to the reference standard (**Fig. 1A**). A reliable
260 feature of HSC cells *in vitro* is expression of two positive markers, fibulin-2 and vascular
261 endothelial-cadherin (VE-Cad) [45]. Our results showed that all HSC cell strains robustly expressed
262 fibulin-2 (**Fig. 1B**) and VE-Cad (**Fig. 1C**), comparable to reference HSC cells, with HTM controls
263 being negative for both markers [45]. In culture, HTM cells upregulate myocilin expression following
264 challenge with the corticosteroid dexamethasone [46], whereas this does not occur in HSC cells. We
265 observed that none of the HSC cell strains expressed myocilin regardless of the presence or
266 absence of dexamethasone (**Fig. 1D**), suggesting pure HSC cell preparations devoid of HTM cell
267 contamination.

268 Together, these data suggest that HSC01, HSC02, HSC03, and HSC09 exhibit required key
269 characteristics according to previous publications [5,45] to faithfully identify them as normal HSC
270 cells, comparable to confirmed reference standards.

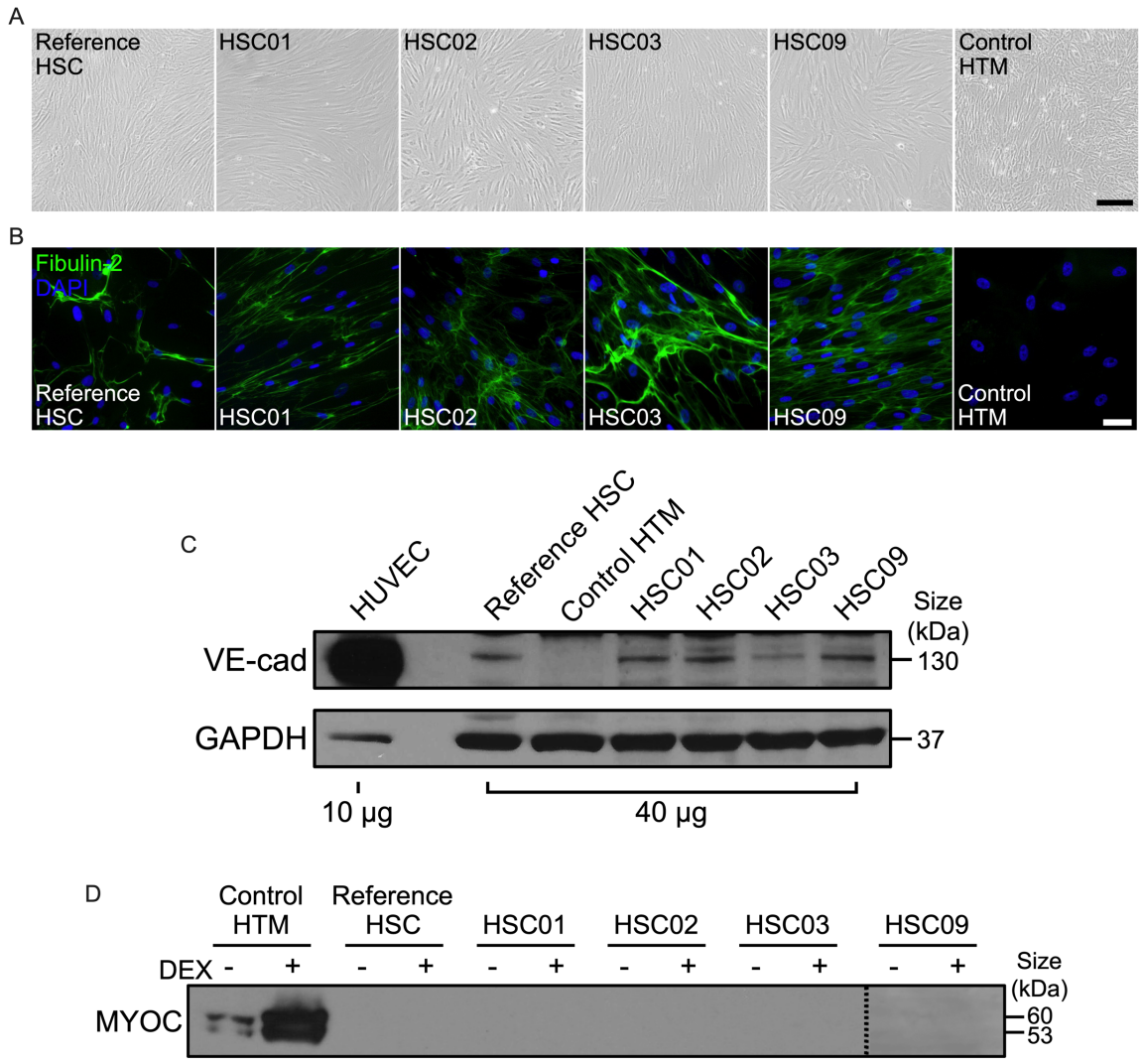

Fig. 1. HSC cell characterization. (A) Representative phase contrast micrographs of reference HSC, HSC01, HSC02, HSC03 and HSC09 cell strains, with HTM controls. Scale bar, 200 µm. (B) Representative immunofluorescence micrographs of fibulin-2. Scale bar, 100 µm. (C) Immunoblot of VE-Cadherin (VE-Cad), with human umbilical vein endothelial (HUVEC) cells serving as positive control. (D) Immunoblot of secreted myocilin (MYOC) without or with dexamethasone (DEX) stimulation at 7 d (= negative marker). Reference HSC cells were provided by K.M.P./W.D.S.. Control HTM cells were previously characterized in ref [43].

Effects of TGFβ2 in the absence or presence of ROCK inhibition or Lat B on actin cytoskeleton in HSC cells.

F-actin stress fibers are found in higher numbers in SC cells isolated from POAG eyes compared to normal SC cells [15]. Moreover, it has been shown that glaucomatous SC cells

284 occasionally exhibit disorganized or "tangled" F-actin fibers; these abnormal cytoskeletal
285 structures often appear as dense groups of actin bundles with multidirectional orientation and
286 overlaps [47]. To investigate the effects of TGFβ2 on actin cytoskeleton remodeling, HSC cells were
287 cultured atop premade ECM hydrogels and treated with TGFβ2 alone or co-treated with ROCK
288 inhibitor Y27632 or latrunculin B (Lat B), a compound that inhibits actin polymerization (**Fig.**
289 **2A**). We observed significantly increased F-actin stress fibers/overall intensity and qualitatively
290 more disorganized F-actin filaments in HSC cells treated with TGFβ2 compared to controls, which
291 was significantly prevented by co-treatment with Y27632 or Lat B, with short Lat B treatment for
292 only 30 min showing a stronger effect (**Fig. 2B,C**). Of note, both types of actin destabilizers failed
293 to fully block TGFβ2-induced F-actin assembly. We observed a range of responsiveness to the
294 TGFβ2 challenge ± treatments among the HSC cell strains, indicating normal donor-to-donor
295 viability.

296 We, and others, have shown that the fibrotic marker α-smooth muscle actin (αSMA) is
297 upregulated in HTM cells by TGFβ2 exposure [28-30,48]. Here, we demonstrated that TGFβ2 induced
298 expression of αSMA in 45.87% of HSC cells compared to only ~3.16% in controls. Similar to
299 results with F-actin, Y27632 prevented αSMA stress fiber formation induced by TGFβ2, with only
300 13.98% αSMA^{+} cells. Interestingly, short-term Lat B treatment failed to block TGFβ2-induced
301 αSMA expression (% of αSMA^{+} cells: 41.95%) (**Fig. 2D,E**).

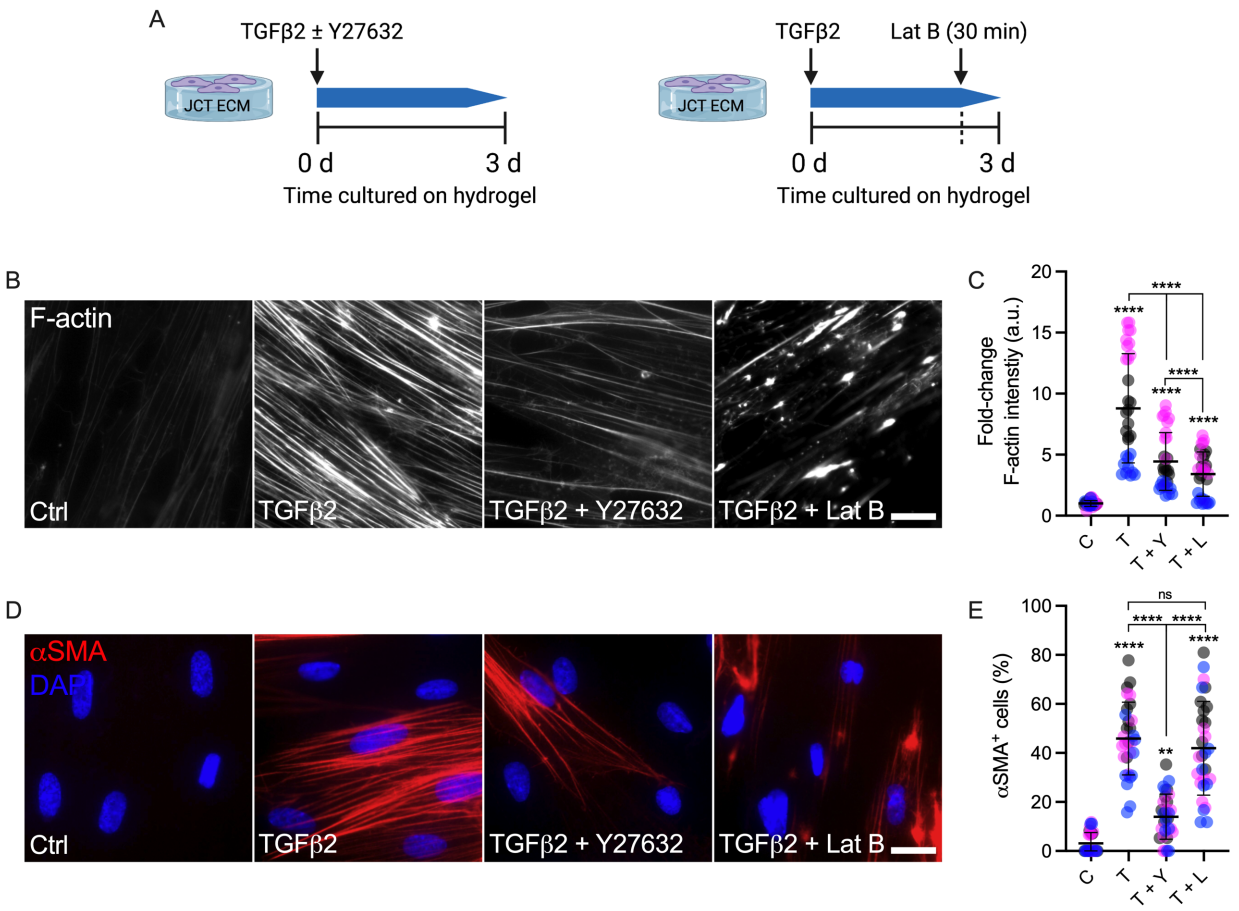

Fig. 2. Effects of TGFβ2 in the absence or presence of a ROCK inhibitor or Lat B on F-actin and αSMA stress fibers in HSC cells. (A) Schematic showing time course of the different treatments. (B) Representative fluorescence micrographs of F-actin in HSC cells on ECM hydrogel substrates subjected to control, TGFβ2 (3 d; 2.5 ng/mL), TGFβ2 + Y27632 (3 d; 10 μM), TGFβ2 (3 d) + Lat B (30 min; 2 μM). Scale bar, 20 μm. (C) Analysis of F-actin intensity (N = 30 images per group from 3 HSC cell strains with 3 replicates per HSC cell strain). (D) Representative immunofluorescence micrographs of αSMA in HSC cells on ECM hydrogel substrates subjected to the different treatments. Scale bar, 20 μm. (E) Analysis of percentage of αSMA$^+$ cells (N = 30 images per group from 3 HSC cell strains with 3 experimental replicates per HSC cell strain; more than 150 cells were analyzed per cell strain). Symbols with different colors represent different cell strains. The bars and error bars indicate Mean ± SD. Significance was determined by two-way ANOVA using multiple comparisons tests (**p<0.01, ****p < 0.0001. ns = non-significant).

To ascertain that the results seen with concurrent exposure to TGFβ2 + Y27632 were not affected by waning inhibitor activity over the 3-day period, HSC cells were treated with TGFβ2 for 3 d followed by supplementation of Y27632 for only 30 min (**Fig. 3A**) to match the Lat B

320 treatment regimen. We observed that HSC cells undergoing short-term ROCK inhibition with
321 Y27632 fully blocked TGFβ2-induced F-actin stress fiber formation, restoring control levels (**Fig.**
322 **3B,C**). As such, ROCK inhibition for only 30 min appeared comparatively more potent than 3 d
323 co-treatment (**Fig. 2B,C**). We also found that short-term supplementation of Y27632 significantly
324 decreased expression of αSMA induced by TGFβ2 (**Fig. 3D,E**), consistent with the 3 d co-
325 treatment data (**Fig. 2B,C**); yet, intensity levels remained significantly higher than controls.

326 Collectively, these data demonstrate that TGFβ2 promotes F-actin stress fiber formation in
327 HSC cells, which is decreased by either actin cytoskeleton relaxation or depolymerization.
328 Furthermore, TGFβ2 induces αSMA expression, which is prevented by ROCK inhibition, even as
329 short as 30 min, whereas short-term actin depolymerization does not influence aberrant αSMA
330 stress fiber formation across different HSC cell strains.

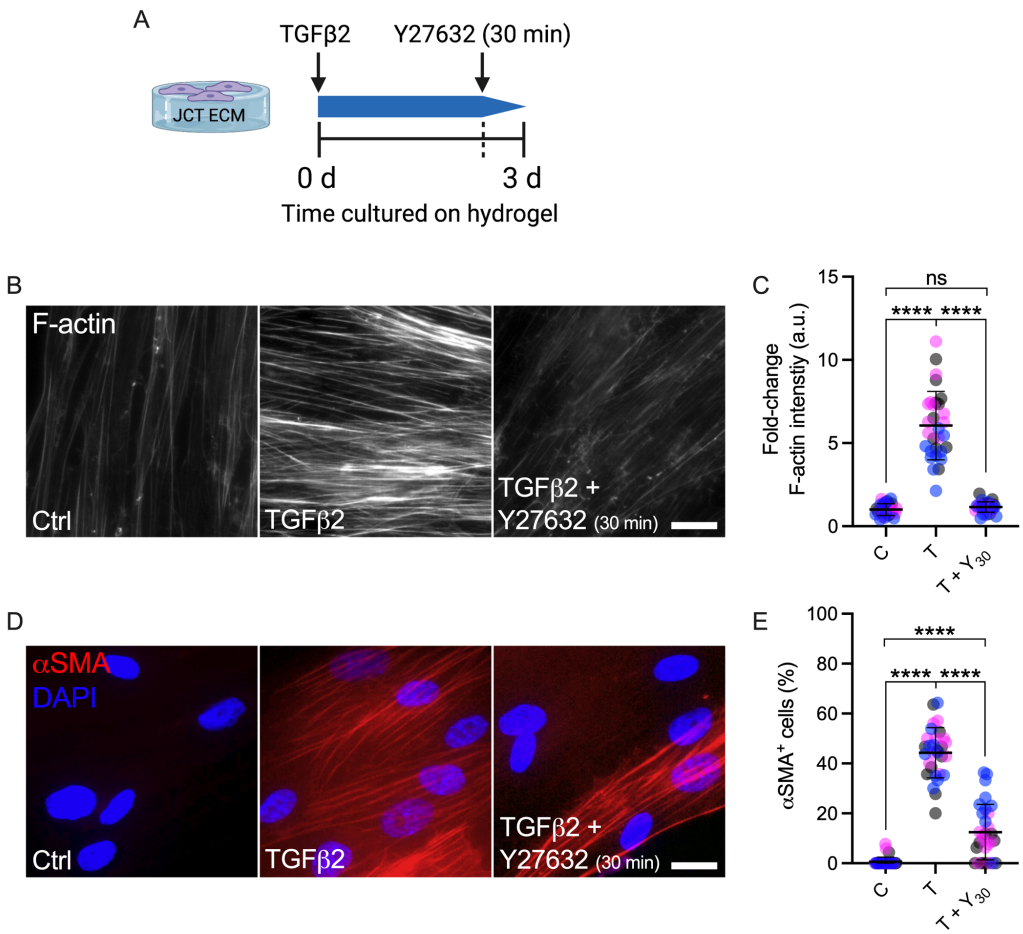

Fig. 3. Effects of short-term ROCK inhibition on TGFβ2-induced F-actin and αSMA stress fibers in HSC cells. (A) Schematic showing time course of short-term ROCK inhibition. (B) Representative fluorescence micrographs of F-actin in HSC cells on ECM hydrogel substrates subjected to control, TGFβ2 (3 d; 2.5 ng/mL), TGFβ2 (3 d) + Y27632 (30 min; 10 μM). Scale bar, 20 μm. (C) Analysis of F-actin intensity (N = 30 images per group from 3 HSC cell strains with 3 replicates per HSC cell strain). (D) Representative immunofluorescence micrographs of αSMA in HSC cells on ECM hydrogel substrates subjected to the different treatments. Scale bar, 20 μm. (E) Analysis of percentage of αSMA^{+} cells (N = 30 images per group from 3 HSC cell strains with 3 experimental replicates per HSC cell strain; more than 150 cells were analyzed per cell strain). Symbols with different colors represent different cell strains. The bars and error bars indicate Mean ± SD. Significance was determined by two-way ANOVA using multiple comparisons tests (****$p < 0.0001$, ns = non-significant).

346 ***TGFβ2 stabilizes actin cytoskeleton to upregulate YAP/TAZ activity***

347 Recently, we demonstrated that TGFβ2 increases nuclear YAP and TAZ, a readout for active
348 YAP/TAZ signaling, in HTM cells cultured atop or within ECM hydrogels [26]. To assess the effect
349 of TGFβ2 on YAP/TAZ subcellular localization in HSC cells subjected to the different treatments,
350 we evaluated both YAP and TAZ nuclear-to-cytoplasmic (N/C) ratios. We observed that exposure
351 to TGFβ2 significantly increased YAP N/C ratio (**Fig. 4A,B**), TAZ N/C ratio (**Fig. 4C,D**) and
352 expression of their putative downstream effector TGM2 (**Fig. 4E,F**) compared to controls,
353 suggesting that TGFβ2 enhanced YAP/TAZ transcriptional activity. Given that actin cytoskeletal
354 integrity is required for proper YAP/TAZ regulation in a variety of cells [41,49], we investigated
355 whether TGFβ2-induced YAP/TAZ activation in HSC cells depended on an intact actin
356 cytoskeleton. Our results revealed that HSC cells co-treated with Y27632 or Lat B significantly
357 decreased TGFβ2-induced YAP/TAZ nuclear localization and TGM2 expression. Consistent with
358 our observation on F-actin fibers in response to the different treatments, Lat B was more effective
359 in decreasing YAP/TAZ activity in HSC cells (i.e., below control levels) compared to Y27632
360 (**Fig. 4A-F**).

361 Together, these data show that TGFβ2 increases nuclear YAP/TAZ and TGM2 expression in
362 HSC cells from multiple donors, which is potently attenuated by either actin cytoskeleton
363 relaxation or depolymerization.

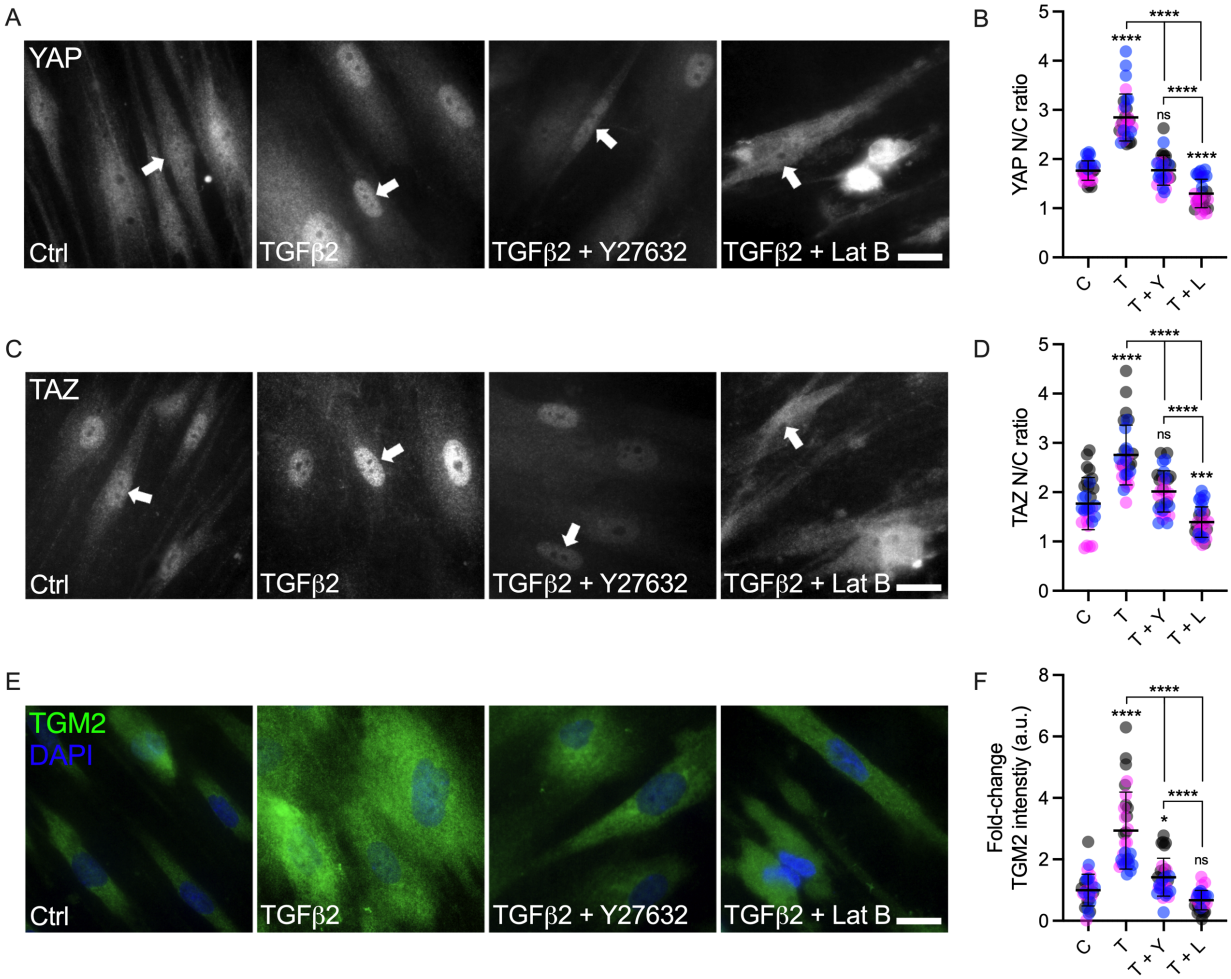

364

365 **Fig. 4. Effects of TGFβ2 in the absence or presence of a ROCK inhibitor or Lat B on**
366 **YAP/TAZ activity in HSC cells.** (A and B) Representative immunofluorescence micrographs of
367 YAP and TAZ in HSC cells on ECM hydrogel substrates subjected to control, TGFβ2 (3 d; 2.5
368 ng/mL), TGFβ2 + Y27632 (3 d; 10 μM), TGFβ2 (3 d) + Lat B (30 min; 2 μM). Arrows indicate
369 YAP/TAZ nuclear localization. Scale bar, 20 μm. (C and D) Analysis of YAP/TAZ
370 nuclear/cytoplasmic ratio (N = 30 images from 3 HSC cell strains with 3 experimental replicates
371 per cell strain). (E) Representative fluorescence micrographs of TGM2 in HSC cells on ECM
372 hydrogel substrates subjected to the different treatments. Scale bar, 20 μm. (F) Analysis of TGM2
373 intensity (N = 30 images from 3 HSC cell strains with 3 replicates per cell strain). Symbols with
374 different colors represent different cell strains. The bars and error bars indicate Mean ± SD.
375 Significance was determined by two-way ANOVA using multiple comparisons tests (*$p<0.05$,
376 ****$p < 0.0001$, ns = non-significant).

377

378

379 ***YAP/TAZ mediate ECM remodeling and actomyosin cell cytoskeleton***

380 It has been shown that HSC cells isolated from glaucomatous eyes exhibit increased F-actin
381 stress fibers and expression of ECM proteins including fibronectin [15]; in this study, our results
382 suggest that TGFβ2 also increases actin cytoskeleton remodeling. Both abnormal ECM deposition
383 and actin remodeling may be part of a pathologic signature in HSC cells. Therefore, we next tested
384 whether pharmacologic YAP/TAZ inhibition could rescue TGFβ2-induced HSC cell dysfunction.
385 To do so, HSC cells atop ECM hydrogels were treated with TGFβ2 alone or co-treated with
386 verteporfin (without light stimulation), which disrupts nuclear YAP/TAZ-TEAD interactions
387 thereby inhibiting transcriptional activity [50]. Co-treatment with TGFβ2 + verteporfin significantly
388 decreased N/C ratios of YAP and TAZ in HSC cells compared to TGFβ2 alone, approximating
389 baseline levels, in agreement with our recent data using HTM cells [51] (**Suppl. Fig. 1A-D**).
390 Similarly, verteporfin significantly decreased TGFβ2-stimulated TGM2 expression; yet, levels
391 remained significantly higher compared to controls (**Suppl. Fig. 1E,F**).

392 We observed that exposure to verteporfin significantly reduced TGFβ2-induced fibronectin
393 deposition approximating untreated controls (**Fig. 5A,B**). Importantly, we demonstrated that
394 TGFβ2-induced αSMA expression (**Fig. 5C,D**), F-actin stress fiber formation (**Fig. 5E,F**), and
395 phospho-myosin light chain (p-MLC) levels (**Fig. 5G,H**) were significantly decreased by
396 verteporfin co-treatment, but again did not reach baseline levels.

397 In sum, these data suggest that pharmacologic YAP/TAZ inhibition reduces the expression of
398 fibronectin and decreases actomyosin cytoskeletal rearrangement across different HSC cell strains.

399

400

401

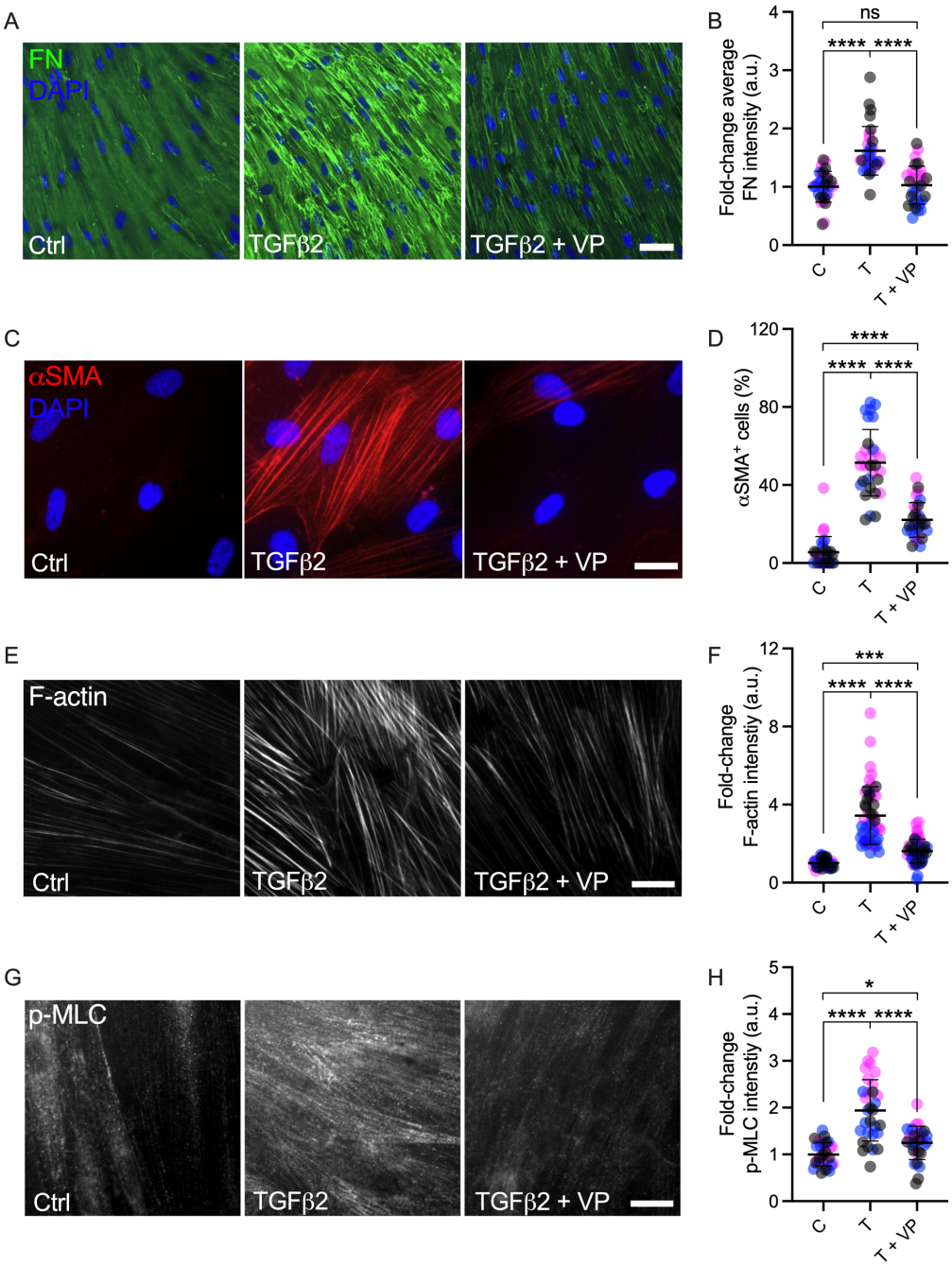

Fig. 5. Effects of pharmacologic YAP/TAZ inhibition on ECM remodeling and actomyosin cytoskeleton in HSC cells. (A) Representative immunofluorescence micrographs of fibronectin (FN) in HSC cells on ECM hydrogel substrates subjected to control, TGFβ2 (3 d; 2.5 ng/mL), TGFβ2 + verteporfin (3 d; 0.5 μM). Scale bar, 100 μm. (B) Analysis of fibronectin intensity (N = 30 images per group from 3 HSC cell strains with 3 experimental replicates per HSC cell strain). (C) Representative immunofluorescence micrographs of αSMA in HSC cells on ECM hydrogel substrates subjected to the different treatments. Scale bar, 20 μm. (D) Analysis of percentage of

411 αSMA$^+$ cells (N = 3 HSC cells strains, more than 150 cells were analyzed per cell strain). (E and
412 G) Representative fluorescence micrographs of F-actin and p-MLC in HSC cells on ECM hydrogel
413 substrates subjected to the different treatments. Scale bar, 20 µm. (F and H) Analysis of F-actin
414 and p-MLC intensity (N = 30 images from 3 HSC cell strains with 3 experimental replicates per
415 cell strain). Symbols with different colors represent different cell strains. The bars and error bars
416 indicate Mean ± SD. Significance was determined by two-way ANOVA using multiple
417 comparisons tests (*$p<0.05$, ***$p<0.001$, ****$p < 0.0001$, ns = non-significant).
418

419 ***YAP/TAZ mediate TGFβ2-induced HSC cell contractility***

420 It has been shown that perfusing *ex vivo* human anterior segments with TGFβ2 reduced the
421 length of the SC inner wall [27], suggestive of tissue contraction. HSC cells are known to be highly
422 contractile [3]. In support of this notion, we observed that HSC cell-laden hydrogels - an
423 experimental tool developed in our laboratory to characterize HTM cell behavior [26,30,43] - in
424 absence of any treatment significantly contracted over time, reaching ~35-42% of their original
425 size by 5 d with normal donor-to-donor variability (**Suppl. Fig.2**).

426 Our data so far showed that YAP/TAZ inhibition reduced pathologic actomyosin cytoskeleton
427 remodeling. Therefore, we hypothesized that TGFβ2 may increase HSC cell contractility, which
428 could be reduced by YAP/TAZ inhibition. To test this hypothesis, we again encapsulated HSC
429 cells in ECM hydrogels and treated the constructs with TGFβ2, either alone or in combination with
430 verteporfin (without light stimulation), to assess the level of hydrogel contraction at 5 d. TGFβ2-
431 treated HSC hydrogels exhibited significantly greater contraction compared to controls (62.79%
432 of controls; **Fig. 6A,B**), consistent with our previous studies using HTM cells [26,30,43]. Co-treatment
433 with verteporfin significantly decreased pathologic HSC hydrogel contraction (81.56% of
434 controls) compared to TGFβ2-treated samples (**Fig. 6A,B**), but it did not fully restore baseline
435 levels. Of note, the influence of verteporfin on HSC cell-laden hydrogel contraction differed
436 between HSC cell strains, showing a stronger effect on HSC02 than HSC03 and HSC09 in line
437 with normal donor-to-donor variability (**Fig. 5A,B**). To rule out that hydrogel contractility was

438 influenced by the cell number, we assessed HSC cell viability in constructs subjected to the
439 different treatments. No differences were observed for HSC cell-laden hydrogels across groups
440 (**Fig. 6C**).

441 Together, these data demonstrate that TGFβ2 robustly induces HSC cell contractility in a 3D
442 ECM microenvironment across multiple cell strains, and that pharmacologic YAP/TAZ inhibition
443 potently decreases pathologic HSC cell contraction.

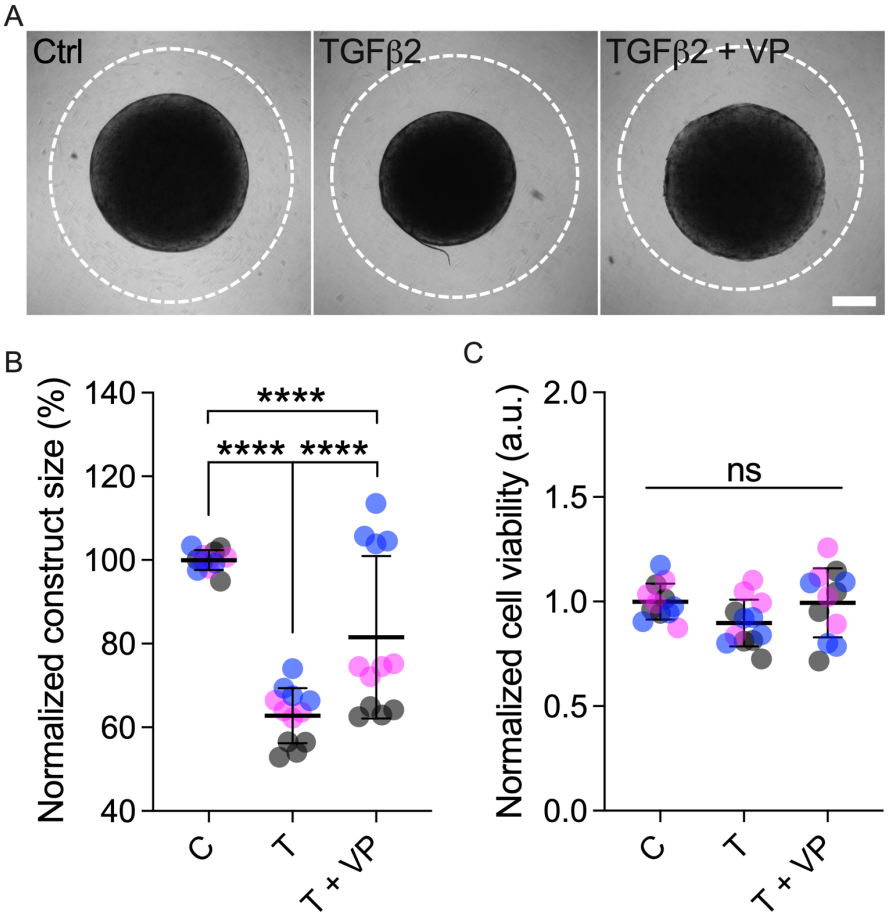

444

445 **Fig. 6. Effects of TGFβ2 in the absence or presence of YAP/TAZ inhibition on HSC hydrogel**
446 **contractility.** (A) Representative brightfield images of HSC hydrogels subjected to control,
447 TGFβ2 (3 d; 2.5 ng/mL), TGFβ2 + verteporfin (3 d; 0.5 μM) at 5 d. Dashed lines outline original
448 size of constructs at 0 d. Scale bar, 1 mm. (B) Construct size quantification of HSC hydrogels
449 subjected to the different treatments at 5 d (N = 12 hydrogels per group from 3 HSC cell strains
450 with 4 experimental replicates per HSC cell strain). (C) Cell viability quantification of HSC
451 hydrogels subjected to the different treatments at 5 d (N = 12 hydrogels per group from 3 HSC cell

452 strains with 4 experimental replicates per HTM cell strain). Symbols with different colors represent
453 different cell strains. The bars and error bars indicate Mean ± SD. Significance was determined by
454 two-way ANOVA using multiple comparisons tests (****p<0.0001, ns = non-significant).

455

456 **Discussion**

457 The profibrotic cytokine TGFβ2 is a key contributor to outflow tissue dysfunction in POAG
458 [10,19]. TGFβ2 has been shown to increase the deposition of ECM material in the JCT-TM beneath
459 the SC inner wall endothelium and contract the SC [26,27,30]. Most *in vitro* studies to date
460 investigating the effects of TGFβ2 on outflow cell dysfunction have focused on TM cells [26,30,48].
461 In contrast, the contributions of TGFβ2 to SC cell pathobiology are considerably less well
462 understood. A recent multi-ethnic genome wide meta-analysis identified *YAP1* as a potential
463 genetic risk factor for POAG, implicating that YAP (and perhaps TAZ by association) may play a
464 critical role in glaucoma pathogenesis [40]. We have shown that TGFβ2 upregulates YAP/TAZ
465 activity in HTM cells cultured atop or within ECM hydrogels [26]. Here, our aim was to elucidate
466 mechanisms governing YAP/TAZ modulation in HSC cells in response to TGFβ2 by culturing
467 cells on a tissue-mimetic ECM substrate.

468 Glaucomatous SC cells isolated from POAG eyes have been shown to exhibit more F-actin
469 stress fibers with an overall higher degree of disorganization compared to normal cells [15].
470 Consistent with this observation, we found that TGFβ2 significantly increased F-actin stress fiber
471 formation in HSC cells with qualitatively more disorganized filaments (**Fig. 2B,C**). Concurrent
472 actin destabilization with Y27632 or Lat B potently decreased TGFβ2-induced actin stress fibers,
473 with short-term Lat B exposure (30 min; necessary to preserve HSC cell viability) showing a
474 stronger effect compared to ROCK inhibitor co-treatment for the full 3 days. When Y27632 was
475 supplemented for only 30 min (i.e., matching the Lat B regimen) to allow for a more accurate side-
476 by-side comparison of the two compounds, an even greater inhibitory effect on pathologic F-actin

477 stress fiber formation was observed (30 min: ~80.94%; 3 d: ~49.55% vs. TGFβ2; **Fig. 2B,C** and
478 **Fig. 3B,C**). These data raise the possibility that by day 3, Y27632 may have lost some of its
479 potency; this would be in line with the reported Y27632 half-life of ~12-16 h [52]. Nevertheless, it
480 is important to note that despite potentially weakened ROCK inhibitory activity, co-treatment of
481 TGFβ2 + Y27632 significantly decreased pathologic F-actin disorganization in HSC cells. It has
482 been extensively reported that the glaucoma-associated stressors dexamethasone and TGFβ2
483 stimulate the formation of cross-linked actin networks (CLANs) in HTM cells [53-56]. In this study,
484 we did not observe any such structures in HSC cells independent of the treatment applied. A
485 number of signaling pathways including Smad, Wnt, ROCK and ERK have been shown to
486 modulate CLAN formation in HTM cells [57]. Further research will be necessary to investigate the
487 specific contribution of these important signaling pathways in HSC cell pathobiology in the
488 context of cytoskeletal homeostasis and remodeling.

489 The transcriptional coactivators YAP and TAZ play important roles in mechanotransduction
490 and POAG pathogenesis [40,41]. Recently, we showed that activity of YAP/TAZ is upregulated in
491 HTM cells under diverse simulated glaucomatous conditions [26]. However, the mechanisms
492 underlying YAP/TAZ signaling in HSC cells influenced by TGFβ2 remain to be elucidated. We
493 here demonstrated that TGFβ2 increased YAP/TAZ nuclear localization and activity in HSC cells,
494 which was potently attenuated by actin cytoskeleton relaxation using Y27632 or actin
495 depolymerization using Lat B (**Fig. 4**). This suggests that actin integrity is required for YAP/TAZ
496 activation in HSC cells. We found that Lat B treatment was more effective in blocking TGFβ2-
497 induced YAP/TAZ nuclear accumulation (i.e., more cytoplasmic YAP/TAZ) than ROCK
498 inhibition with Y27632, consistent with the F-actin stress fiber data. A previous study showed that
499 HTM cells can recover to their initial state after removal of Lat B treatment in a short period of

500 time [58]. It would be worthwhile to further investigate whether Y27632/Lat B-reduced YAP/TAZ
501 activity could be reversed with the treatments withheld.

502 Endothelial-to-mesenchymal transition (EndMT) is a process whereby endothelial cells
503 undergo a series of molecular events, such as increased expression of αSMA, fibronectin,
504 vimentin, and collagen types I and III, that lead to a change in phenotype toward mesenchymal-
505 like cells [59,60]. TGFβ has been shown to induce EndMT, which can contribute to various fibrotic
506 diseases and cancers [60-63]. In a previous study, it was shown that TGFβ2 stimulated EndMT of
507 HSC cells cultured on top of a synthetic biomaterial; downregulation of endothelial cell markers
508 and upregulation of mesenchymal makers were noted [64]. Consistent with this, we showed that
509 TGFβ2 enhanced EndMT of HSC cells cultured atop tissue-mimetic ECM hydrogels, as indicated
510 by increased formation of fibronectin and αSMA (**Fig. 2D,E, Fig. 3D,E, Fig. 5A-D**). The TGFβ2-
511 induced αSMA stress fibers were potently disrupted by short-term exposure to Y27632. We
512 measured a ~71.84% decrease in αSMA-positive cells with only 30-min of ROCK inhibition
513 compared to TGFβ2-treated HSC cells, nearly identical to the full 3 d co-treatment (~69.52%). By
514 contrast, Lat B-mediated actin depolymerization failed to reduce αSMA-positive cells.
515 Importantly, we found that TGFβ2-induced EndMT in HSC cells was potently blocked by
516 pharmacologic YAP/TAZ inhibition with verteporfin in absence of light stimulation consistent
517 with previous reports in non-ocular [65-67] and ocular cells [51,68,69]; significantly decreased fibronectin
518 and actin stress fibers were noted (**Fig. 5A-D**). Moreover, TAP/TAZ inhibition decreased TGFβ2-
519 induced expression of TGM2 (**Suppl. Fig. 1E,F**), which crosslinks fibronectin and thereby stiffens
520 the ECM [70]. This suggests that YAP/TAZ inhibition may decrease ECM stiffness to improve
521 aqueous humor outflow. Therefore, targeting YAP/TAZ signaling in the SC endothelium to inhibit
522 EndMT is an intriguing strategy for managing ocular hypertension.

523 Actomyosin, the actin-myosin complex, regulates cell contractility in various cell types [71]
524 including HSC cells [3]. To that end, HSC cells in absence of any treatment exhibited qualitatively
525 fewer F-actin fibers compared to HTM cells when cultured atop our ECM hydrogels. Therefore,
526 we speculate that the higher degree of HSC cell contractility could stem from upregulated activity
527 of myosin II, which is responsible for producing contraction force [72]. Myosin II activity is primarily
528 regulated by phosphorylation of MLC; this process is mediated by myosin light chain kinase
529 (MLCK) and myosin phosphatase [73]. Importantly, MLCK inhibition has been shown to decrease
530 IOP in rabbit eyes [74]. Blebbistatin, a pharmacologic inhibitor of myosin II adenosine triphosphatase
531 activity, increases outflow facility via blocking the binding of myosin to actin [75]. Futures studies
532 would be necessary to investigate in greater detail the role of myosin II activity and myosin-actin
533 interactions in HSC cell biology.

534 Consistent with our observation on HTM cells, TGFβ2-treated HSC cells exhibited elevated
535 levels of cell contractility-related molecules (i.e., αSMA, F-actin and p-MLC), which correlated
536 with increased HSC hydrogel contraction. Importantly, this TGFβ2-induced pathologic process
537 was potently attenuated by pharmacologic YAP/TAZ inhibition (**Fig. 5C-H, Fig. 6B-D**). Previous
538 studies showed that outflow resistance is modulated by SC cell stiffness, which is directly
539 correlated with their contractility status [14,76]. It would be worthwhile to further investigate the
540 effects of YAP/TAZ inhibition on HSC cell stiffness.

541 In conclusion, by culturing HSC cells on tissue-mimetic ECM hydrogels, we demonstrated that
542 TGFβ2 drives actin stress fiber formation to upregulate YAP/TAZ activity, and that YAP/TAZ
543 inhibition reduces HSC cell contractility, which may positively affect cell stiffness and outflow
544 resistance. Our findings provide new evidence for a pathologic role of YAP/TAZ hyperactivation

545 in HSC cell pathobiology in glaucoma, and suggest that pharmacologic YAP/TAZ inhibition has
546 promising potential to improve outflow tissue dysfunction.
547
548 **Disclosure**
549 The authors report no conflicts of interest.
550
551 **Funding**
552 This project was supported in part by National Institutes of Health grants R01EY022359
553 and P30EY005722 (W.D.S.) and K08EY031755 (P.S.G), an American Glaucoma Society Young
554 Clinician Scientist Award (to P.S.G.), a Syracuse University BioInspired Seed Grant (to S.H.),
555 unrestricted grants to SUNY Upstate Medical University Department of Ophthalmology and
556 Visual Sciences from Research to Prevent Blindness (RPB) and from Lions Region 20-Y1, and
557 RPB Career Development Awards (to P.S.G. and S.H.).
558
559 **Acknowledgments**
560 We thank Dr. Robert W. Weisenthal and the team at Specialty Surgery Center of Central
561 New York for assistance with corneal rim specimens. We also thank Dr. Nasim Annabi at the
562 University of California – Los Angeles for providing the KCTS-ELP, Dr. Alison Patteson at
563 Syracuse University for rheometer access, and Drs. Audrey M. Bernstein and Mariano S. Viapiano
564 at SUNY Upstate Medical University for imaging support. **Author contributions:** H.L., A.S.,
565 K.M.P., W.D.S., P.S.G., and S.H. designed all experiments, collected, analyzed, and interpreted
566 the data. K.M.P. and W.D.S. provided the HSC reference cells. H.L. and S.H. wrote the

manuscript. All authors commented on and approved the final manuscript. P.S.G. and S.H. conceived and supervised the research. **Data and materials availability:** All data needed to evaluate the conclusions in the paper are present in the paper and/or the Supplementary Materials. Additional data related to this paper may be requested from the authors.

References

1. Ashpole NE, Overby DR, Ethier CR, Stamer WD. Shear stress-triggered nitric oxide release from Schlemm's canal cells. *Investigative ophthalmology & visual science* 2014;55:8067-8076.
2. Dautriche CN, Tian Y, Xie Y, Sharfstein ST. A Closer Look at Schlemm's Canal Cell Physiology: Implications for Biomimetics. *J Funct Biomater* 2015;6:963-985.
3. Stamer WD, Braakman ST, Zhou EH, et al. Biomechanics of Schlemm's canal endothelium and intraocular pressure reduction. *Prog Retin Eye Res* 2015;44:86-98.
4. Ethier CR. The inner wall of Schlemm's canal. *Exp Eye Res* 2002;74:161-172.
5. Stamer WD, Roberts BC, Howell DN, Epstein DL. Isolation, culture, and characterization of endothelial cells from Schlemm's canal. *Invest Ophthalmol Vis Sci* 1998;39:1804-1812.
6. Gong H, Francis AW. Schlemm s Canal and Collector Channels as Therapeutic Targets. 2014.
7. Tamm ER. The trabecular meshwork outflow pathways: structural and functional aspects. *Exp Eye Res* 2009;88:648-655.
8. Tamm ER, Braunger BM, Fuchshofer R. Intraocular Pressure and the Mechanisms Involved in Resistance of the Aqueous Humor Flow in the Trabecular Meshwork Outflow Pathways. *Prog Mol Biol Transl Sci* 2015;134:301-314.
9. Brubaker RF. Flow of aqueous humor in humans [The Friedenwald Lecture]. *Invest Ophthalmol Vis Sci* 1991;32:3145-3166.
10. Quigley HA. Open-angle glaucoma. *N Engl J Med* 1993;328:1097-1106.
11. Quigley HA, Broman AT. The number of people with glaucoma worldwide in 2010 and 2020. *Br J Ophthalmol* 2006;90:262-267.
12. Kwon YH, Fingert JH, Kuehn MH, Alward WL. Primary open-angle glaucoma. *N Engl J Med* 2009;360:1113-1124.
13. Tham YC, Li X, Wong TY, Quigley HA, Aung T, Cheng CY. Global prevalence of glaucoma and projections of glaucoma burden through 2040: a systematic review and meta-analysis. *Ophthalmology* 2014;121:2081-2090.
14. Overby DR, Zhou EH, Vargas-Pinto R, et al. Altered mechanobiology of Schlemm's canal endothelial cells in glaucoma. *Proc Natl Acad Sci U S A* 2014;111:13876-13881.
15. Kelly RA, Perkumas KM, Campbell M, et al. Fibrotic Changes to Schlemm's Canal Endothelial Cells in Glaucoma. *Int J Mol Sci* 2021;22.
16. Tian YI, Zhang X, Torrejon K, et al. A bioengineering approach to Schlemm's canal-like stem cell differentiation for in vitro glaucoma drug screening. *Acta Biomater* 2020;105:203-213.

607 17. Rao PV, Deng PF, Kumar J, Epstein DL. Modulation of aqueous humor outflow facility
608 by the Rho kinase-specific inhibitor Y-27632. *Invest Ophthalmol Vis Sci* 2001;42:1029-1037.
609 18. Kumar J, Epstein DL. Rho GTPase-mediated cytoskeletal organization in Schlemm's
610 canal cells play a critical role in the regulation of aqueous humor outflow facility. *J Cell*
611 *Biochem* 2011;112:600-606.
612 19. Fuchshofer R, Tamm ER. Modulation of extracellular matrix turnover in the trabecular
613 meshwork. *Experimental Eye Research* 2009;88:683-688.
614 20. Granstein RD, Staszewski R, Knisely TL, et al. Aqueous humor contains transforming
615 growth factor-beta and a small (less than 3500 daltons) inhibitor of thymocyte proliferation. *J*
616 *Immunol* 1990;144:3021-3027.
617 21. Inatani M, Tanihara H, Katsuta H, Honjo M, Kido N, Honda Y. Transforming growth
618 factor-beta 2 levels in aqueous humor of glaucomatous eyes. *Graefes Arch Clin Exp Ophthalmol*
619 2001;239:109-113.
620 22. Agarwal P, Daher AM, Agarwal R. Aqueous humor TGF-β2 levels in patients with open-
621 angle glaucoma: A meta-analysis. *Molecular vision* 2015;21:612-620.
622 23. Kasetti RB, Maddineni P, Patel PD, Searby C, Sheffield VC, Zode GS. Transforming
623 growth factor β2 (TGFβ2) signaling plays a key role in glucocorticoid-induced ocular
624 hypertension. *J Biol Chem* 2018;293:9854-9868.
625 24. Ochiai Y, Ochiai H. Higher concentration of transforming growth factor-beta in aqueous
626 humor of glaucomatous eyes and diabetic eyes. *Jpn J Ophthalmol* 2002;46:249-253.
627 25. Picht G, Welge-Luessen U, Grehn F, Lutjen-Drecoll E. Transforming growth factor beta
628 2 levels in the aqueous humor in different types of glaucoma and the relation to filtering bleb
629 development. *Graefes Arch Clin Exp Ophthalmol* 2001;239:199-207.
630 26. Li H, Raghunathan V, Stamer WD, Ganapathy PS, Herberg S. Extracellular Matrix
631 Stiffness and TGFβ2 Regulate YAP/TAZ Activity in Human Trabecular Meshwork Cells.
632 *Frontiers in Cell and Developmental Biology* 2022;10.
633 27. Gottanka J, Chan D, Eichhorn M, Lutjen-Drecoll E, Ethier CR. Effects of TGF-beta2 in
634 perfused human eyes. *Invest Ophthalmol Vis Sci* 2004;45:153-158.
635 28. Han H, Wecker T, Grehn F, Schlunck G. Elasticity-Dependent Modulation of TGF-β
636 Responses in Human Trabecular Meshwork Cells. *Investigative Ophthalmology & Visual*
637 *Science* 2011;52:2889-2896.
638 29. Pattabiraman PP, Rao PV. Mechanistic basis of Rho GTPase-induced extracellular matrix
639 synthesis in trabecular meshwork cells. *Am J Physiol Cell Physiol* 2010;298:C749-763.
640 30. Li H, Henty-Ridilla JL, Bernstein AM, Ganapathy PS, Herberg S. TGFβ2 regulates
641 human trabecular meshwork cell contractility via ERK and ROCK pathways with distinct
642 signaling crosstalk dependent on the culture substrate. *Current Eye Research* 2022;1-41.
643 31. Fuchshofer R, Welge-Lussen U, Lütjen-Drecoll E. The effect of TGF-beta2 on human
644 trabecular meshwork extracellular proteolytic system. *Exp Eye Res* 2003;77:757-765.
645 32. Fuchshofer R, Tamm ER. The role of TGF-β in the pathogenesis of primary open-angle
646 glaucoma. *Cell Tissue Res* 2012;347:279-290.
647 33. Welge-Lüßen U, May CA, Lütjen-Drecoll E. Induction of Tissue Transglutaminase in the
648 Trabecular Meshwork by TGF-β1 and TGF-β2. *Investigative Ophthalmology & Visual Science*
649 2000;41:2229-2238.
650 34. Moroishi T, Hansen CG, Guan K-L. The emerging roles of YAP and TAZ in cancer.
651 *Nature Reviews Cancer* 2015;15:73-79.

652 35. Plouffe SW, Hong AW, Guan K-L. Disease implications of the Hippo/YAP pathway.
653 *Trends in Molecular Medicine* 2015;21:212-222.
654 36. Polansky JR, Fauss DJ, Zimmerman CC. Regulation of TIGR/MYOC gene expression in
655 human trabecular meshwork cells. *Eye (Lond)* 2000;14 (Pt 3B):503-514.
656 37. Zhao B, Wei X, Li W, et al. Inactivation of YAP oncoprotein by the Hippo pathway is
657 involved in cell contact inhibition and tissue growth control. *Genes Dev* 2007;21:2747-2761.
658 38. Silver JS, Günay KA, Cutler AA, et al. Injury-mediated stiffening persistently activates
659 muscle stem cells through YAP and TAZ mechanotransduction. *Sci Adv* 2021;7.
660 39. Low BC, Pan CQ, Shivashankar GV, Bershadsky A, Sudol M, Sheetz M. YAP/TAZ as
661 mechanosensors and mechanotransducers in regulating organ size and tumor growth. *FEBS Lett*
662 2014;588:2663-2670.
663 40. Gharahkhani P, Jorgenson E, Hysi P, et al. Genome-wide meta-analysis identifies 127
664 open-angle glaucoma loci with consistent effect across ancestries. *Nat Commun* 2021;12:1258.
665 41. Dupont S, Morsut L, Aragona M, et al. Role of YAP/TAZ in mechanotransduction.
666 *Nature* 2011;474:179-183.
667 42. Boopathy GTK, Hong W. Role of Hippo Pathway-YAP/TAZ Signaling in Angiogenesis.
668 *Frontiers in Cell and Developmental Biology* 2019;7.
669 43. Li H, Bague T, Kirschner A, et al. A tissue-engineered human trabecular meshwork
670 hydrogel for advanced glaucoma disease modeling. *Exp Eye Res* 2021;205:108472.
671 44. Sapudom J, Müller CD, Nguyen KT, Martin S, Anderegg U, Pompe T. Matrix
672 Remodeling and Hyaluronan Production by Myofibroblasts and Cancer-Associated Fibroblasts
673 in 3D Collagen Matrices. *Gels* 2020;6.
674 45. Perkumas KM, Stamer WD. Protein markers and differentiation in culture for Schlemm's
675 canal endothelial cells. *Exp Eye Res* 2012;96:82-87.
676 46. Keller KE, Bhattacharya SK, Borras T, et al. Consensus recommendations for trabecular
677 meshwork cell isolation, characterization and culture. *Exp Eye Res* 2018;171:164-173.
678 47. Read AT, Chan DW, Ethier CR. Actin structure in the outflow tract of normal and
679 glaucomatous eyes. *Exp Eye Res* 2007;84:214-226.
680 48. Torrejon KY, Papke EL, Halman JR, et al. TGFβ2-induced outflow alterations in a
681 bioengineered trabecular meshwork are offset by a rho-associated kinase inhibitor. *Sci Rep*
682 2016;6:38319.
683 49. Das A, Fischer RS, Pan D, Waterman CM. YAP Nuclear Localization in the Absence of
684 Cell-Cell Contact Is Mediated by a Filamentous Actin-dependent, Myosin II- and Phospho-YAP-
685 independent Pathway during Extracellular Matrix Mechanosensing*. *Journal of Biological*
686 *Chemistry* 2016;291:6096-6110.
687 50. Liu-Chittenden Y, Huang B, Shim JS, et al. Genetic and pharmacological disruption of
688 the TEAD-YAP complex suppresses the oncogenic activity of YAP. *Genes Dev* 2012;26:1300-
689 1305.
690 51. Li H, Raghunathan V, Stamer WD, Ganapathy PS, Herberg S. Extracellular Matrix
691 Stiffness and TGFbeta2 Regulate YAP/TAZ Activity in Human Trabecular Meshwork Cells.
692 *Front Cell Dev Biol* 2022;10:844342.
693 52. Mertsch S, Oellers P, Wendling M, Stracke W, Thanos S. Dissecting the inter-substrate
694 navigation of migrating glioblastoma cells with the stripe assay reveals a causative role of
695 ROCK. *Mol Neurobiol* 2013;48:169-179.
696 53. Montecchi-Palmer M, Bermudez JY, Webber HC, Patel GC, Clark AF, Mao W. TGFβ2
697 Induces the Formation of Cross-Linked Actin Networks (CLANs) in Human Trabecular

698 Meshwork Cells Through the Smad and Non-Smad Dependent Pathways. *Investigative*
699 *ophthalmology & visual science* 2017;58:1288-1295.
700 54. Clark AF, Brotchie D, Read AT, et al. Dexamethasone alters F-actin architecture and
701 promotes cross-linked actin network formation in human trabecular meshwork tissue. *Cell Motil*
702 *Cytoskeleton* 2005;60:83-95.
703 55. Yuan Y, Call MK, Yuan Y, et al. Dexamethasone Induces Cross-Linked Actin Networks
704 in Trabecular Meshwork Cells Through Noncanonical Wnt Signaling. *Investigative*
705 *Ophthalmology & Visual Science* 2013;54:6502-6509.
706 56. Filla MS, Schwinn MK, Nosie AK, Clark RW, Peters DM. Dexamethasone-associated
707 cross-linked actin network formation in human trabecular meshwork cells involves beta3 integrin
708 signaling. *Invest Ophthalmol Vis Sci* 2011;52:2952-2959.
709 57. Zhang YE. Non-Smad pathways in TGF-β signaling. *Cell Research* 2009;19:128-139.
710 58. McKee CT, Wood JA, Shah NM, et al. The effect of biophysical attributes of the ocular
711 trabecular meshwork associated with glaucoma on the cell response to therapeutic agents.
712 *Biomaterials* 2011;32:2417-2423.
713 59. Choi KJ, Nam J-K, Kim J-H, Choi S-H, Lee Y-J. Endothelial-to-mesenchymal transition
714 in anticancer therapy and normal tissue damage. *Exp Mol Med* 2020;52:781-792.
715 60. Ma J, Sanchez-Duffhues G, Goumans M-J, ten Dijke P. TGF-β-Induced Endothelial to
716 Mesenchymal Transition in Disease and Tissue Engineering. *Frontiers in Cell and*
717 *Developmental Biology* 2020;8.
718 61. Clere N, Renault S, Corre I. Endothelial-to-Mesenchymal Transition in Cancer. *Frontiers*
719 *in Cell and Developmental Biology* 2020;8.
720 62. Zeisberg EM, Potenta SE, Sugimoto H, Zeisberg M, Kalluri R. Fibroblasts in kidney
721 fibrosis emerge via endothelial-to-mesenchymal transition. *J Am Soc Nephrol* 2008;19:2282-
722 2287.
723 63. Pérez L, Muñoz-Durango N, Riedel CA, et al. Endothelial-to-mesenchymal transition:
724 Cytokine-mediated pathways that determine endothelial fibrosis under inflammatory conditions.
725 *Cytokine Growth Factor Rev* 2017;33:41-54.
726 64. Dautriche CN, Szymanski D, Kerr M, et al. A biomimetic Schlemm's canal inner wall: A
727 model to study outflow physiology, glaucoma pathology and high-throughput drug screening.
728 *Biomaterials* 2015;65:86-92.
729 65. Jang M, An J, Oh SW, et al. Matrix stiffness epigenetically regulates the oncogenic
730 activation of the Yes-associated protein in gastric cancer. *Nat Biomed Eng* 2021;5:114-123.
731 66. Mason DE, Collins JM, Dawahare JH, et al. YAP and TAZ limit cytoskeletal and focal
732 adhesion maturation to enable persistent cell motility. *J Cell Biol* 2019;218:1369-1389.
733 67. Wei C, Li X. Verteporfin inhibits cell proliferation and induces apoptosis in different
734 subtypes of breast cancer cell lines without light activation. *BMC Cancer* 2020;20:1042.
735 68. Chen WS, Cao Z, Krishnan C, Panjwani N. Verteporfin without light stimulation inhibits
736 YAP activation in trabecular meshwork cells: Implications for glaucoma treatment. *Biochem*
737 *Biophys Res Commun* 2015;466:221-225.
738 69. Murphy R, Irnaten M, Hopkins A, et al. Matrix Mechanotransduction via Yes-Associated
739 Protein in Human Lamina Cribrosa Cells in Glaucoma. *Invest Ophthalmol Vis Sci* 2022;63:16.
740 70. Akimov SS, Krylov D, Fleischman LF, Belkin AM. Tissue transglutaminase is an
741 integrin-binding adhesion coreceptor for fibronectin. *The Journal of cell biology* 2000;148:825-
742 838.

743 71. Murrell M, Oakes PW, Lenz M, Gardel ML. Forcing cells into shape: the mechanics of
744 actomyosin contractility. *Nat Rev Mol Cell Biol* 2015;16:486-498.
745 72. Kolega J. The role of myosin II motor activity in distributing myosin asymmetrically and
746 coupling protrusive activity to cell translocation. *Mol Biol Cell* 2006;17:4435-4445.
747 73. Fukata Y, Amano M, Kaibuchi K. Rho-Rho-kinase pathway in smooth muscle
748 contraction and cytoskeletal reorganization of non-muscle cells. *Trends Pharmacol Sci*
749 2001;22:32-39.
750 74. Honjo M, Inatani M, Kido N, et al. A myosin light chain kinase inhibitor, ML-9, lowers
751 the intraocular pressure in rabbit eyes. *Exp Eye Res* 2002;75:135-142.
752 75. Zhang M, Rao PV. Blebbistatin, a Novel Inhibitor of Myosin II ATPase Activity,
753 Increases Aqueous Humor Outflow Facility in Perfused Enucleated Porcine Eyes. *Investigative*
754 *Ophthalmology & Visual Science* 2005;46:4130-4138.
755 76. Zhou EH, Krishnan R, Stamer WD, et al. Mechanical responsiveness of the endothelial
756 cell of Schlemm's canal: scope, variability and its potential role in controlling aqueous humour
757 outflow. *J R Soc Interface* 2012;9:1144-1155.
758